Available online at www.sciencedirect.com

SciVerse ScienceDirect

Acta Materialia 60 (2012) 977–983

Acta MATERIALIA

www.elsevier.com/locate/actamat

Source-based strengthening of sub-micrometer Al fibers

Frédéric Mompiou [a], Marc Legros [a,*], Andreas Sedlmayr [b], Daniel S. Gianola [c], Daniel Caillard [a], Oliver Kraft [b]

[a] CEMES – Centre d'Elaboration des Matériaux et d'Etudes Structurales–CNRS Toulouse, France
[b] Institut fur Angewandte Materialien, Karlsruhe Institute for Technology, Karlsruhe, Germany
[c] Department of Material Sciences and Engineering, University of Pennsylvania, Philadelphia, PA, USA

Received 30 September 2011; received in revised form 3 November 2011; accepted 3 November 2011

Abstract

The origin of the improved mechanical properties of sub-micron single crystals and whiskers is still debated, but studies generally concentrate solely on size effects. In comparison, the role of the initial defect content, linked to the crystal size, has been given less consideration. We show using in situ SEM and TEM tensile testing of sub-micron Al fibers prepared using selective etching of a eutectic alloy that multiplication of dislocations through intermittent spiral sources directly causes a power-law increase of the yield stress with decreasing cross-sectional size. The size effect and resulting mechanical response are directly linked to the initial defect density and the distance between the source and the surface. In the absence of dislocations, fibers elastically reach high stresses with limited to no plasticity, reminiscent of whisker behavior.

Keywords: In situ scanning electron microscopy (SEM); In situ transmission electron microscopy (TEM); Size effect; Mechanical properties; Aluminum fibers

1. Introduction

The strength of metals and alloys is inversely dependent on the ability of their dislocations to multiply and travel over large distances inside the crystalline lattice. When reduced to very small dimensions, metallic crystals become much more resistant to plastic deformation, as revealed by classic experiments on whiskers [1,2] and recent tests on micropillars [3]. Despite widely scattered yield stresses [4], focused ion beam (FIB) prepared micropillars and wires demonstrate a clear trend of strengths that scale as a power law of their size. These size effects were found to differ strongly when considering the crystal structure (body-centered cubic (bcc) [5,6] or face-centered cubic (fcc) [7,8]) or the mode of testing [9], questioning the physical origin of this power law dependence. Because of nearby free surfaces, dislocations may easily escape the crystal, provoking a starvation of plastic deformation [10]. In situ TEM experiments conducted in compression tend to confirm this hypothesis [11], while others in tension show a constant dislocation density throughout plastic deformation [12]. Dislocation multiplication through statistically dispersed spiral sources could induce a hardening [13]. Such spiral sources were found to operate in discrete dislocation dynamics (DDD) simulations [14,15] but their stability is questioned by atomistic calculations in crystals smaller than 50 nm in diameter. Plastic deformation would therefore require surface nucleation of dislocations to sustain plastic flow [16]. The high strength of whiskers is due to the perfection of such crystals that do not initially contain dislocations. They fail at stresses sufficient to nucleate a crack or dislocations from the surface, which approach the theoretical strength limit. Because this stress depends on the atomic roughness of the surface, it may exhibit only weak intrinsic size dependence [17,18]. Bei et al. showed that short sub-micron Mo-based alloy pillars, not prepared by FIB, which were initially dislocation-free, could reach theoretical strength regardless of their diameter [19]. Their strength dropped by nearly 90% and "regular"

* Corresponding author. Tel.: +33 5 62 25 78 42; fax: +33 5 62 25 79 99.
E-mail address: legros@cemes.fr (M. Legros).

1359-6454/$36.00 © 2011 Acta Materialia Inc. Published by Elsevier Ltd. All rights reserved.
doi:10.1016/j.actamat.2011.11.005

size-dependent plasticity was recovered when pre-straining the fibers in the eutectic alloy or when illuminating them with Ga ions in the FIB [20]. The strength and mechanical behavior of small crystals therefore appear dependent on their initial defect content and on their size. If one considers a given bulk defect density, sampling a diminishingly small volume should statistically lead to defect-free crystals. This perspective strongly hinges on the preparation route, and the FIB approach, like other fabrication methods, could lead to damage structures that need to be considered prior to testing [21–23]. The lack of quantitative information about the initial defect content and character, however, shrouds a complete understanding of small-scale plasticity in uncertainty.

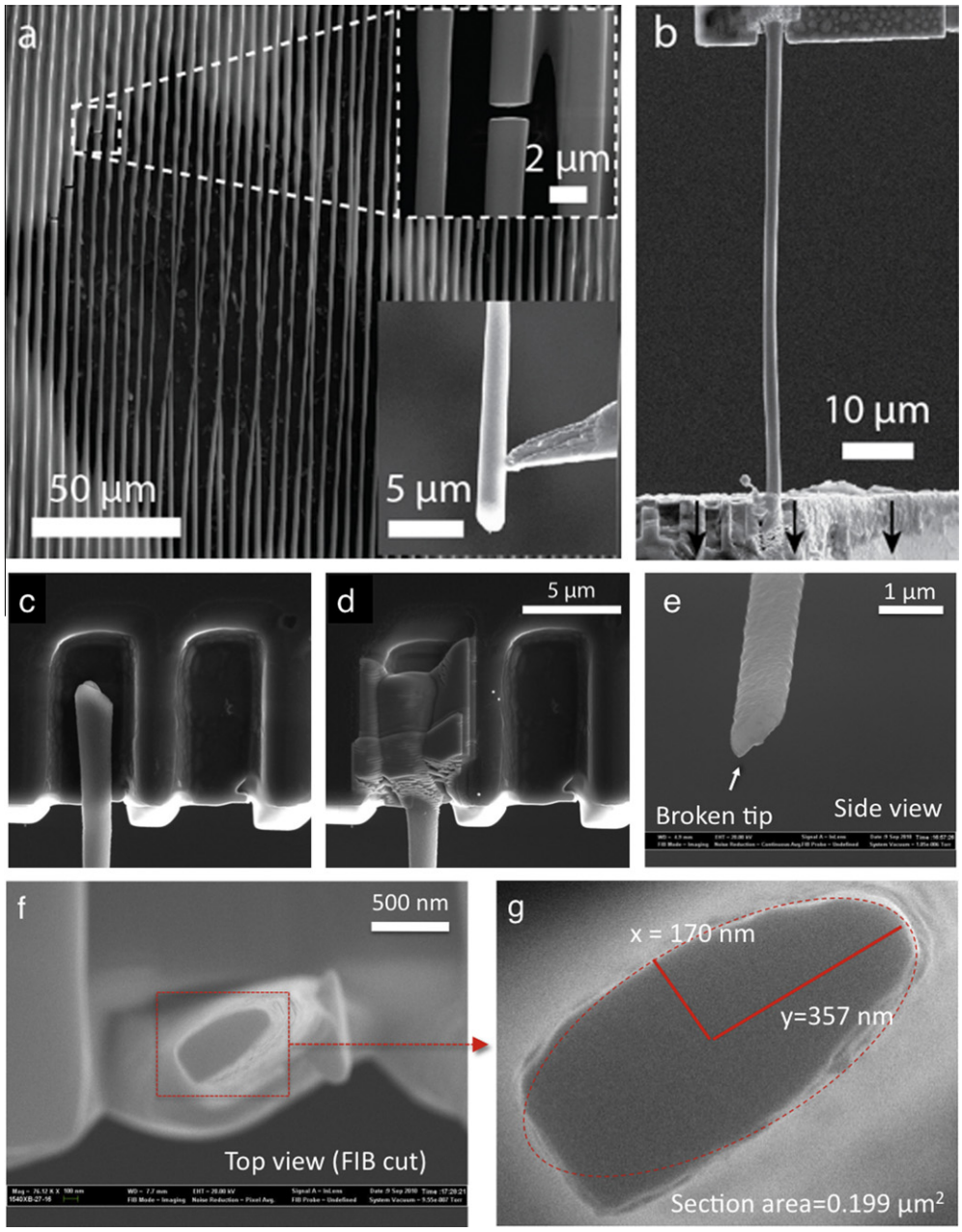

Fig. 1. Al fibers exposed after differential etching of an Al/Al_2Cu lamellar eutectic (a) SEM image (boxes are zooms of FIB cuts and micromanipulation of an individual fiber). Individual fiber testing set-up inside the SEM using a micro-load cell and a micromanipulator (b). Black arrows indicate the straining direction. Gripping of individual fibers before tensile testing starts with the lowering of fiber ends into FIB-cut troughs (c), followed by the deposition of a continuous Pt-layer (d) between the grips and the fiber, creating a strong bond. Cross-section measurement of Al fibers after SEM testing (e–g). A FIB cut is made perpendicular to the fiber at the location of the plastically deformed (and broken) tip (e), the tip is then viewed end-on (f), and from this view, the semi-major (noted y) and semi-minor diameter (noted x and taken as the scale parameter in this study) of the elliptical section can be retrieved (g). The section area is determined from (g) using pixel counting in image processing software.

2. Experimental

In the present work, Al fibers were fabricated using preferential etching of an Al/Al_2Cu lamellar eutectic. The resulting in situ samples consisted of millimeter-size rectangles, containing free-standing submicron Al fibers aligned along the longest direction of the sample (Fig. 1a). These fibers were single-crystalline Al with effective diameters ranging from 120 nm to 1.2 μm, and some showed an apparent residual Cu content of 1–3 wt.%, in the error range of the measurement technique (EDX). Weak beam imaging and microdiffraction investigations revealed that the fibers were totally free of Cu precipitates, suggesting that impurities were in solid solution in Al or segregated to the external surfaces of the fibers [24] because of the low solubility of Cu in Al at room temperature. In each rectangular sample, chemical etching produced fibers of different lengths, with an elliptical cross-section, generally thinner at their center. These rectangles were stretched as-is in a straining holder for in situ TEM experiments (carried out in a JEOL 2010 operated at 160–200 kV) while individual fibers were harvested individually for quantitative in situ SEM investigations (Fig. 1a and g) [25]. The test performed inside the TEM corresponds to a displacement-controlled experiment.

In situ SEM tensile testing was carried out inside a FEI NovaNanolab 200 dual-beam system equipped with a feedback-enabled displacement control dedicated transducer (Hysitron Inc., $F_{max} = 10$ mN, Resolution $\leqslant 60$ nN) [26] using independently controlled positioning stages (Attocube Systems) [27]. A Kleindiek Nanotechnik micromanipulator and a local e-beam Pt deposition served for the manipulation and welding of individual fibers. One end of the fiber is lowered into a trough connected to nanopositioners (Fig. 1c) and further welded using a combination of e-beam and i-beam induced local Pt-deposition (Fig. 1d). The other side is then cut free from the manipulator, transferred, aligned and welded to the transducer. Nominal strain rates of 10^{-5}–10^{-4} s^{-1} were applied. Data were recorded at rates of 100–500 Hz, depending on the load cell and controller set-up used. When possible, tests were interrupted after a significant amount of plasticity to allow for microstructure inspection with TEM.

Local strain was calculated using digital image correlation (DIC) code written for Matlab, which mitigates the

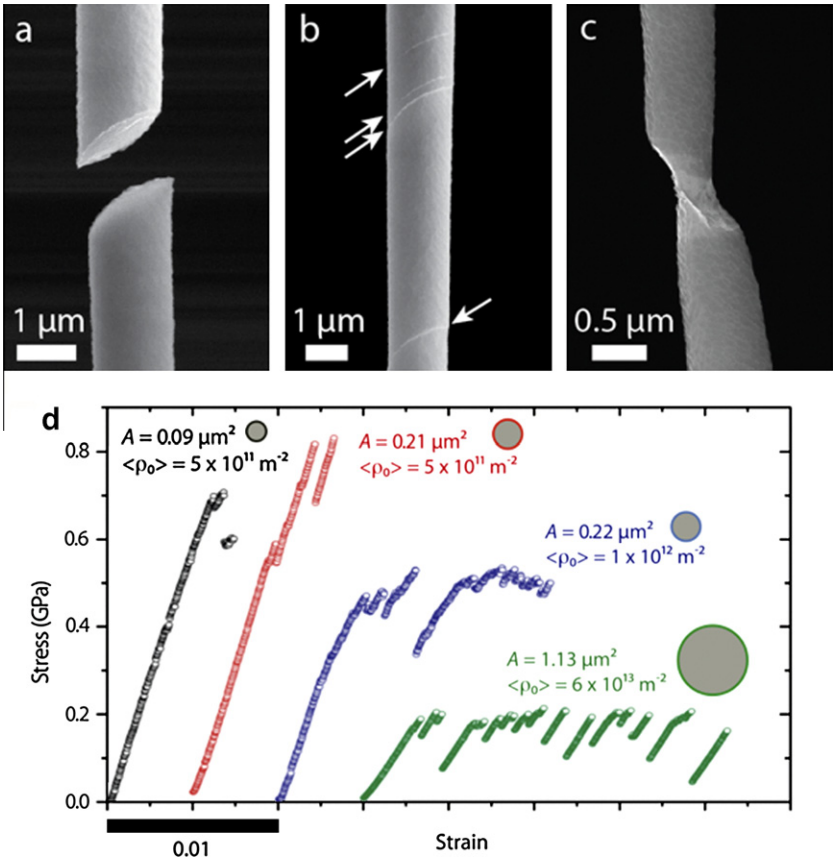

Fig. 2. SEM observations of deformed fibers after test showing brittle failure (a), disperse slip lines (b) and necking (c). Stress–strain plots obtained for fibers with different sections A (illustrated with scaled disks) and average dislocation densities $\langle \rho_0 \rangle$ (d). The black curve shows a whisker-like behavior while green and blue curves exhibit a yield stress followed by significant plasticity, punctuated with load drops. The red curve shows an intermediate behavior (high stress, very little plasticity). Variations in apparent Young's moduli are attributed to the nominal strain being averaged over non-uniform fiber section, while stress values are always calculated in the heavily deformed regions [27]. (For interpretation of the references to colour in this figure legend, the reader is referred to the web version of this article.)

contributions of machine compliance to the apparent strain [28,29]. To calculate the stress from the load values measured during in situ SEM testing, fibers were sectioned with FIB after post-mortem TEM inspection in a region taken as close as possible from the plastically deformed region (Fig. 1e–g) and looked top-down along the fiber axis. As seen in Fig. 1f, fibers have a rather elliptical section, and this procedure permits the determination of the semi-major radius (noted y) and semi-minor radius (noted x and taken here as the scaling parameter) of the elliptical section. At that point, stress can be calculated and combined with strain measurements, leading to stress–strain curves that are shown in Fig. 2d. It is important to note that this method leads to accurate yield stress values, but may induce an apparent deviation from the Young modulus of Al, especially if the fiber displays some important section variations (strain averaging effects [27]) or if plastic deformation occurs in the thinnest section. All fibers which underwent quantitative in situ SEM tensile testing were characterized using TEM both prior to and after testing to determine the full evolution of dislocation densities and arrangement.

3. Results and discussion

Representative stress–strain curves for Al fibers of varying cross-sectional sizes (A) and initial dislocation density ($\langle\rho_o\rangle$) are shown in Fig. 2d, which shows mechanical response reminiscent of that of both small-scale whiskers and pillars. We define the yield stress as the value corresponding to the first deviation of the linear elastic portion of the curve (Fig. 2d). This deviation often arises as a sharp load drop that is commonly associated with the appearance of slip bands in SEM images (Fig. 2b). Plastic deformation occurs through limited (Fig. 2b) or localized (Fig. 2c) plasticity, although some fibers with very low dislocation density also fail in a brittle manner (Fig. 2a). A striking observation is that two fibers of similar section ($A \sim 0.2\ \mu m^2$, red and blue curves) exhibit very different ultimate strengths and behavior. The blue curve, corresponding to a higher dislocation density, reaches lower stresses but a larger plastic strain (Fig. 2d), while the fiber with lower initial dislocation density maintains stresses over 800 MPa but is not able to undergo large amounts of plastic deformation. In contrast, fibers with different sizes but similar initial dislocation densities ($\langle\rho_o\rangle \sim 5 \times 10^{11}\ m^{-2}$, black and red curves) both show relatively high strength and limited ductility with an apparent softening effect with decreasing size. These measurements emphasize the importance of both size and initial defect density in controlling the mechanical response of these Al fibers.

As discussed in the previous paragraph, knowing the average dislocation density in a given fiber prior to deformation is fundamental information. However, this density is very heterogeneous along the fiber length, so we focused on one fiber section where localized plastic deformation took place to show the evolution and participation of individual dislocations. Fig. 3 represents the microstructure of a 700 nm wide fiber before and after test. To capture the inhomogeneous distribution of dislocations along a given fiber, we have represented both the initial mean density, measured along the whole fiber ($1.7 \times 10^{12}\ m^{-2}$, blue dashed line) and the local dislocation density, taken in 200 nm long fiber sections in the plasticity affected zone (Fig. 3a). We chose this value of 200 nm to discriminate the four dislocations initially present, labeled d_{1-4} in the region that underwent plasticity, necking and fracture. This results in a quantified representation of dislocation density (Fig. 3a). As can be seen in Fig. 3b and c, all the deformation occurred in the region of d_1 leading to a steep density increase while the region of d_{1-3} remained unaffected. Beyond these three dislocations, the density remained nil. No starvation (annihilation of the dislocation density) was observed in the current experiments. On the contrary, we observed the occurrence of multiplication processes in volumes smaller than 1 μm^3. In Fig. 3c, ~20–40 dislocations were produced in a zone where only one dislocation (d_1) was present prior to testing (Fig. 3b).

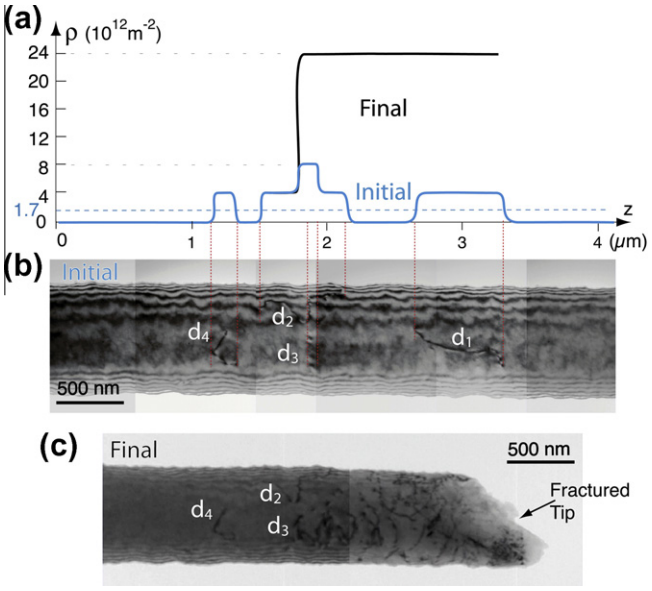

Fig. 3. Typical microstructure found along an Al fiber prior to (b) and after (c) SEM testing. The corresponding dislocation densities (initial (blue curve) and final (black curve)) are represented in (a). The dislocation population increases only in the plastically affected zone, close to the fractured tip. Note that dislocations d_{2-4} remained unaffected. (For interpretation of the references to colour in this figure legend, the reader is referred to the web version of this article.)

In situ TEM tensile tests revealed different behaviors, spanning from abrupt fracture (cleavage along (1 1 1) planes within one video frame = 0.04 s, resulting in fracture surfaces similar to Fig 2a) in fibers that contained very few dislocations, to extensive plasticity dispersed in multiple slip affected zones (similar to those displayed in Figs. 2c and 3c), when the initial density of dislocations was high.

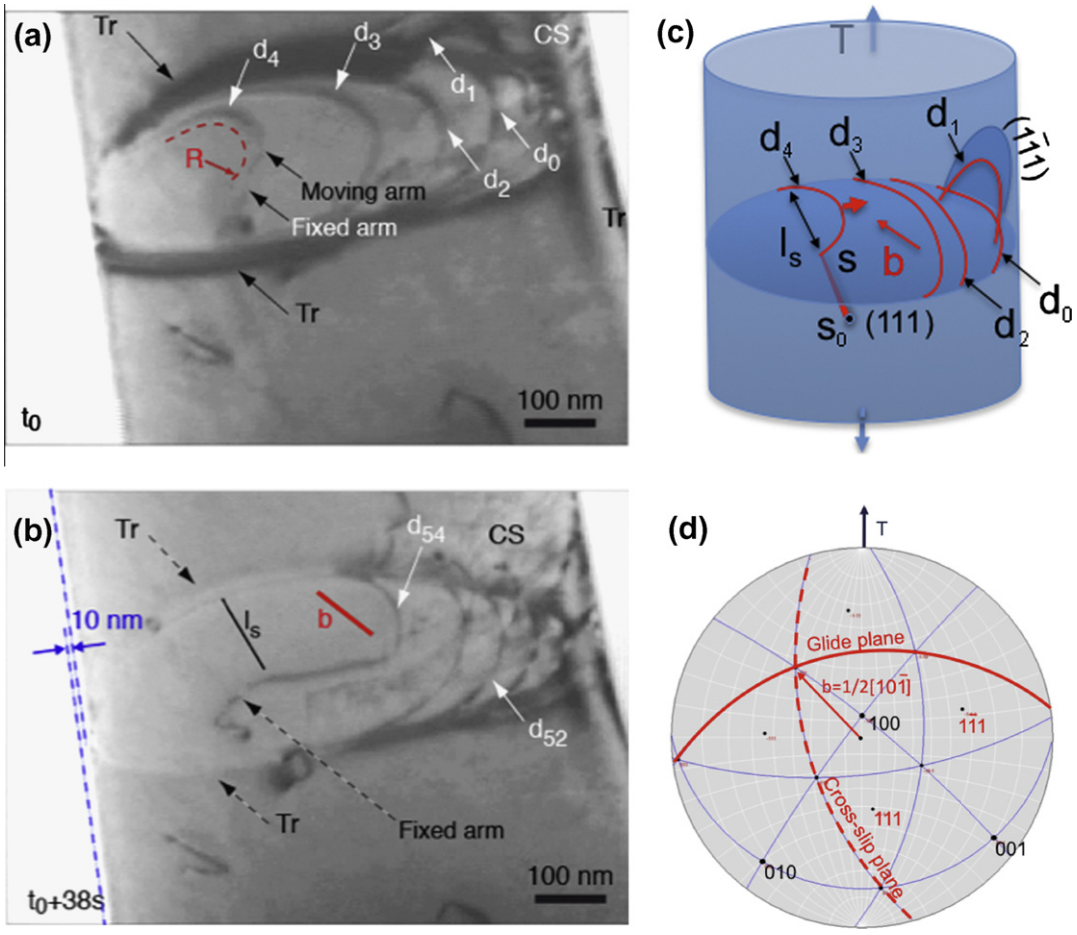

Fig. 4. Single arm source operating for a finite time (54 loop emissions in 38 s). (a) and (b) are video stills that correspond to the source operating and stopping, respectively. Note the dislocation d_1 moving to another glide plane in the cross-slip zone (CS) in (a). (c) is a sketch of the observed configuration. S–S_0 is the fixed arm (S is the rotating point of the source inside the crystal, and S_0 is the connection at the surface), (1 1 1) is the initial glide plane and (1 −1 1) the plane of cross-slip. $\mathbf{b} = \frac{1}{2}[1\,0\,-1]$ is the Burgers vector. These directions and planes are reported on the stereographic projection (d) along with the tensile axis T. The primary (1 1 1) glide plane is inclined 48° from the TEM screen. The Schmid factor is maximal for the source ($s = 0.38$) and lower for the cross-slip (1 −1 1) plane ($s = 0.13$).

Although many initial dislocations remained immobile throughout testing, the first dislocation movements often consisted in dislocation half loops running to the surface, resulting in annihilation or strong reduction of their length. A small fraction of these events led to the activation of single arm (or "spiral") sources on one (single slip) or two (double slip) glide planes. Fig. 4 shows one of these sources operating in a 750 nm wide fiber (see Video S1). In Fig. 4a, the spiral source is captured in operation generating dislocation loops in a (1 1 1) glide plane by turning clockwise around a fixed arm. The moving arm propagates to the right, and forms a dynamical pile-up because of the non-immediate evacuation of dislocations to the free surfaces. Thick and transient slip traces (noted Tr. in Fig. 4a) are evidence of the slow shear of the native oxide by the dislocations. The source being closer to the left side, segments emitted in that direction escape the crystal prior to forming a pile-up. Once the source stops by cross-slipping of the fixed arm, the slip traces are erased, which means that the dislocations have completely escaped the crystal (Fig. 4b). 10–20% of dislocations contained in the pile-up to the right cross slip onto the (1 −1 1) plane (Fig. 4a and b), directly indicating the direction of the Burgers vector **b**. Between each turn, the moving arm stops or significantly slows at a position where the distance l_s between the fixed arm and the surface is the shortest (Fig. 4b and c). This corresponds to a transient equilibrium position, sketched in Fig. 4c, where the dislocation curvature is the smallest. This curvature corresponds to a balance between the line tension of the dislocation and the applied resolved shear stress τ. For a screw dislocation this equilibrium obeys the simplified relation $\tau \approx \mu b/R$, where μ is the shear modulus, and b the magnitude of the Burgers vector [30]. Because the line-tension force increases when the radius of curvature decreases, the transient equilibrium is reached when the dislocation curvature is minimum, i.e. when the distance l_s is minimum ($R \approx l_s/2$). Thus, higher stresses are needed to activate sources with a fixed arm close to the surface. When τ exceeds a critical stress τ_{cr}, R increases, τ decreases, and the dislocation expands and moves freely.

This process repeats itself, resulting in an oscillatory stress cycle with a period matching that of the single-arm windmill motion [15]. Smoother motion of sources corresponds to smaller amplitudes of stress during oscillations, i.e. to dislocation curvatures remaining close to the critical radius of curvature. This is achieved when $l_s \approx x/2$, x being the semi-minor axis of the elliptical section of the fiber (Fig. 1g). Similar spiral sources were observed in differently sized fibers, and a comparable critical position was found in all instances for the moving arm corresponding to the minimization of l_s. In Fig. 4, the fixed arm is located close to the center of the fiber, resulting in smooth emission of dislocations (see Video S1). When the arm is closer to the surface, the stress increases and jerky dislocation emissions are observed (see Video S2). Larger shears in single planes are also observed along the fibers (not shown). During all the observation of spiral sources operating at the onset of plasticity (>20), the moving loops never encountered a hard point that would signify the presence of a precipitate [31]. The stopping point of the moving segment always corresponded to the equilibrium configuration ($R \approx l_s/2$). This, once again, underlines the absence of Cu precipitates or their complete innocuity relative to the dislocation movements. Cross-slip from the initial glide plane was not often observed, and the fact that the Schmid factor for the cross-slip plane was not very high (Fig. 4d) suggests that this deviation from the initial glide plane could be favored by the dense pile-up on the right. The pile-up is probably caused by the native oxide that acts as a damping obstacle to the exit of dislocations at the surface. Dark slip traces (Tr, Fig. 4a) are visible when the source is active, signifying the presence of dislocations inside the crystal. These slip traces are eliminated after a few seconds (absence of Tr, Fig. 4b), suggesting the complete exit of the dislocations from the crystal. As the size of the fiber decreases, the role played by the native oxide may therefore impact the strain rate sensitivity of Al. This effect will be addressed in a future work.

Strain and strain rate can also be accounted for either by counting the dislocation segments emitted (an exact measure) or by measuring the produced shear on the side of the fiber (10 nm in Fig. 4b) that confirms the exit of all dislocation through the surfaces. During source operation, the dislocation density can also be monitored. It remained constant at $\sim 4 \times 10^{14}\ m^{-2}$ during the source operation and dropped to $10^{14}\ m^{-2}$ upon cessation of the source.

The effects of size and dislocation density on yield stress measurements from in situ SEM (single fiber testing, blue and green squares) and in situ TEM testing (dislocation curvature from spiral sources, black dots) are reported in Fig. 5. As expected, the yield stress increases as the inverse of the fiber dimensions (semi-minor axis x) and also as a function of a decrease in dislocation density. As no obvious change in plastic mechanisms was observed in this range of dimensions (150–1500 nm), it is not surprising to observe this tendency both in instrumented SEM experiments and in dislocation-based TEM measurements. The stress

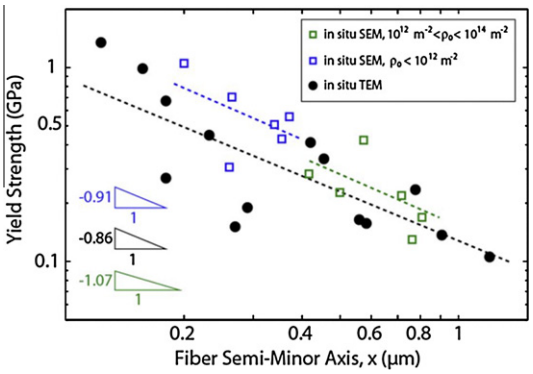

Fig. 5. Flow stresses obtained from in situ SEM straining (open squares) and from dislocation curvature measured during in situ TEM straining (solid circles) as a function of the fiber smallest dimension x (ellipse minor axis). Resolved shear stresses given by dislocation curvatures are converted to yield stresses using Schmid's law. SEM results are sorted between low (blue squares) and high (green squares) initial dislocation density. (For interpretation of the references to colour in this figure legend, the reader is referred to the web version of this article.)

increase (near 1 GPa) represents a significant fraction of the theoretical strength of pure Al estimated using the shear modulus $\mu = 28$ GPa (between $\mu/30$ and $\mu/2\pi$, 0.9–4.1 GPa [32]), which is expected to not be very influenced by the presence of impurities. These stresses are reached even with one dislocation source activated, suggesting that these experiments on fibers with low dislocation density may elucidate the transition from pillar (multiple dislocation interactions, strain hardening) to whisker behavior (surface dislocation nucleation near or at theoretical strength). For fibers with high density (green squares), low density (blue squares) and spiral source measurements (black dots), the power law exponents are found close to -1 (Fig. 5), similar to recent experiments on Al pillars [33] and to the most recent source-based discrete dislocation dynamics simulations that reproduce realistic microstructures [15]. These simulations underline the important scatter introduced by the initial dislocation structures in the mechanical response of micropillars. Indeed, the present in situ TEM experiments showed that a single dislocation could lead to a spiral source and to significant plasticity, but that many initially present dislocations do not necessarily participate in accommodation of plastic strain (also shown in Fig. 3). This effect, combined with the current limited statistical data on the yield stress of small objects, is also in line with the variation of exponents found in the literature: 0.6 for electrodeposited and FIB made fcc micropillars [7,22] to 0.8 for Al pillars [33]. A high initial dislocation density favors only the probability of having one or several dislocation segments that are correctly oriented so they can form active sources and lead to dislocation multiplication. Conversely, a low dislocation density would reduce the probability of having a source. The size effect will therefore appear much more scattered in small crystals with a low dislocation density.

4. Conclusion

Using extrinsic (load cell combined with image correlation for in situ SEM) and intrinsic (dislocation curvature of expanded loops counted individually for in situ TEM) measurements, we can conclude that the onset and development of heterogeneous plasticity in sub-micron-sized aluminum wires depend on the activation of spiral sources. Moreover, the position of these sources relative to the free surface is what governs the yield stress of the individual fiber and thus what dictates the size effect. The closer to the surface the source is, the higher the stress. Once activated, plastic deformation occurs without hardening because dislocations are rapidly eliminated through free surfaces despite a drag effect of the natural oxide. Elimination is much faster in smaller fibers or when the source is closer to the surface (higher stress). In situ SEM and TEM experiments converge to show that the initial microstructure and size controls the yield stress and that a single dislocation source is able to generate large plasticity. As a result, since the source may not approach the surface indefinitely, a strength gap may always separate crystals containing dislocations (pillars, microsamples made by FIB) and those that need to nucleate them from the surface (whiskers).

Acknowledgments

This work was performed in the framework of the ESTEEM European network (esteem.ua.ac.be/). D.S.G. acknowledges partial support from an NSF CAREER Award, NSF-DMR 1056293, and start-up funding from the University of Pennsylvania.

Appendix A. Supplementary data

Supplementary data associated with this article can be found, in the online version, at doi:10.1016/j.actamat.2011.11.005.

References

[1] Brenner SS. J Appl Phys 1958;30:266.
[2] Brenner SS. Science 1958;128:569.
[3] Uchic MD, Dimiduk DM, Florando JN, Nix WD. Science 2004;305:986.
[4] Rinaldi A, Peralta P, Friesen C, Sieradzki K. Acta Mater 2008;56:511.
[5] Schneider AS, Kaufmann D, Clark BG, Frick CP, Gruber PA, Mönig R, et al. Phys Rev Lett 2009;103:105501.
[6] Kim J-Y, Jang D, Greer JR. Acta Mater 2010;58:2355.
[7] Uchic M, Shade P, Dimiduk D. JOM J Miner, Metals Mater Soc 2009;61:36.
[8] Kraft O, Gruber PA, Mönig R, Weygand D. Ann Rev Mater Res 2010;40:296.
[9] Kiener D, Grosinger W, Dehm G, Pippan R. Acta Mater 2008;56:580.
[10] Greer JR, Nix WD. Phys Rev B 2006:73.
[11] Shan ZW, Mishra RK, Asif SAS, Warren OL, Minor AM. Nature Mater 2008;7:115.
[12] Oh SH, Legros M, Kiener D, Dehm G. Nature Mater 2009;8:95.
[13] Parthasarathy TA, Rao SI, Dimiduk DM, Uchic MD, Trinkle DR. Scripta Mater 2007;56:313.
[14] Tang H, Schwarz KW, Espinosa HD. Phys Rev Lett 2008;100:185503.
[15] Motz C, Weygand D, Senger J, Gumbsch P. Acta Mater 2009;57:1744.
[16] Weinberger CR, Cai W. Scripta Mater 2011;64:529.
[17] Hirel P, Godet J, Brochard S, Pizzagalli L, Beauchamp P. Phys Rev B 2008;78:064109.
[18] Zhu T, Li J. Prog Mater Sci 2010;55:710.
[19] Bei H, Shim S, Miller MK, Pharr GM, George EP. Appl Phys Lett 2007;91:111915.
[20] Bei H, Shim S, George EP, Miller MK, Herbert EG, Pharr GM. Scripta Mater 2007;57:397.
[21] Maas R, Van Petegem S, Zimmermann J, Borca CN, Van Swygenhoven H. Scripta Mater 2008;59:471.
[22] Jennings AT, Burek MJ, Greer JR. Phys Rev Lett 2010;104:135503.
[23] Lee G, Kim J-Y, Budiman AS, Tamura N, Kunz M, Chen K, et al. Acta Mater 2010;58:1361.
[24] Bader S, Kalaugher EM, Arzt E. Thin Solid Films 1995;263:175.
[25] Richter G, Hillerich K, Gianola DS, Mönig R, Kraft O, Volkert CA. Nano Lett 2009;9:3048.
[26] Warren OL. PI 85 SEM PicoIndenter with the performech control unit; 2010.
[27] Gianola DS, Sedlmayr A, Mönig R, Volkert CA, Major RC, Cyrankowski E, et al. Rev Sci Instrum 2011;82:063901.
[28] Eberl C, Gianola DS, Thompson R. Digital image correlation and tracking. In: Natick MA, editor. MatLabCentral, Mathworks file exchange server, FileID:12413. The Mathworks, Inc; 2006.
[29] Gianola DS, Eberl C. JOM J Miner, Metals Mater Soc 2009;61:24.
[30] Hirth JP, Lothe J. Theory of dislocations. New York: Wiley; 1982.
[31] Vivas M, Lours P, Levaillant C, Couret A, Casanove M-J, Coujou A. Philos Mag A; 76:921.
[32] Paxton AT, Gumbsch P, Methfessel M. Philos Mag Lett 1991;63:267.
[33] Kaufmann D, Mönig R, Volkert CA, Kraft O. Int J Plast 2011;27:470.